Nano Communication Networks 37 (2023) 100456

Contents lists available at ScienceDirect

Nano Communication Networks

journal homepage: www.elsevier.com/locate/nanocomnet

Evolutionary generative adversarial network based end-to-end learning for MIMO molecular communication with drift system ☆

Jiarui Zhu [a], Chenyao Bai [a,*], Yunlong Zhu [a,*], Xiwen Lu [a], Kezhi Wang [b]

[a] Academy for Engineering and Technology, Fudan University, Shanghai 200433, China
[b] Department of Computer Science, Brunel University London, Kingston Lane, Uxbridge UB8 3PH, UK

ARTICLE INFO

Article history:
Received 5 December 2022
Received in revised form 13 March 2023
Accepted 3 May 2023
Available online 8 May 2023

Keywords:
End-to-end learning
Evolutionary computation
Generative adversarial network
Molecular communication
Multiple-input multiple-output

ABSTRACT

Molecular communication (MC) is a novel paradigm for nano-communication networks. Compared with diffusion-based single-input single-out (SISO) systems, multiple-input multiple-output (MIMO) MC with drift systems can effectively mitigate the negative effects of inter symbol interference (ISI), inter link interference (ILI) and noise, further improving transmission efficiency. The modeling complexity of MIMO MC systems inspires the application of deep learning (DL) techniques to establish end-to-end architectures for signal recovery. However, training of the entire end-to-end system is limited by the unknown channel and small training sample size. In this paper, aiming at signal recovery of the newly developed mathematical MIMO MC with drift system model, a Kullback–Leibler divergence (KLD) evolutionary generative adversarial network (EGAN)-based end-to-end learning method is proposed. The end-to-end architecture can be trained offline with both the sampled and fake signals generated by KLD EGAN, even with a small training sample size, and then used to recover online transmitted signals directly. Besides, two traditional detection algorithms denoted as the maximum a posterior (MAP) detector and fixed threshold (FT) detector, are proposed as well for theoretical comparison. Experiments of the effect of different model parameters on the system performance have been carried out. Results validate the effectiveness and robustness of our proposed method compared to other DL-based methods, including the deep neural networks (DNN)-based, the original GAN-based, and the original EGAN-based, in terms of transmission accuracy.

1. Introduction

In most conventional communication systems, information is transmitted via electromagnetic signals. In this case, an analytical channel model can be formulated, and signal detection can be carried out based on it [1]. However, with the emergence of new communication scenarios, sometimes the mathematical channel model is challenging to achieve due to complex perceptual processes, especially for molecular communication (MC). MC is a biologically inspired technology utilizing molecules to communicate between nano-transceivers [2]. Typically, at the transmitter node, information is encoded into the chemical or physical properties of specific molecules, which then propagates through the channel and is finally received and decoded by the receiver node. There exist three main architectures to characterize the molecular propagation process: walkway-based, flow-based, and diffusion-based [3]. Compared with conventional electromagnetic wave-based communication, MC has advantages in terms of energy efficiency, power consumption, and bio-compatibility. Thus, it has great potential in various fields such as environmental monitoring [4], advanced materials design [5], and targeted drug delivery systems [6].

The slow and uncertain propagation of molecules in single-input single-output (SISO) MC model creates a long-tail effect that leads to inter-symbol interference (ISI) in molecular reception and reduces transmission efficiency. Multiple-input multiple-output (MIMO) technology can effectively increase the data transmission rate and has become one of the most promising key technologies in communication transmission. In [7], possible advantages of applying MIMO to MC system and prospective directions for future progress are discussed. The world's first molecular MIMO communication link was implemented in [8], demonstrating that MIMO can achieve data rates about 1.7 times higher than those of SISO molecular communication systems. However, with multiple links in MIMO model, inter link interference (ILI) becomes a newly introduced communication interference, defined as the reception by the receiver of molecules sent from non-corresponding transmitters. Signal detection at the receiver node

☆ This work was supported by China Postdoctoral Science Foundation (Grant No. 2021M690701).

* Corresponding authors.
E-mail addresses: baichenyao@fudan.edu.cn (C. Bai), zyl@fudan.edu.cn (Y. Zhu).

https://doi.org/10.1016/j.nancom.2023.100456
1878-7789/

would be more challenging with the joint effect of ILI and ISI since this will lead to the channel model hard to model. Some novel detection algorithms for MC with a 2×2 MIMO configuration are developed for receiver design in [9]. Authors in [10] proposed two algorithms to solve the formulated optimization problems and further optimized a 3×3 MIMO receiver.

In most communication systems, modules are designed separately, such as source encoder, channel encoder, modulator, demodulator, channel decoder, source decoder, etc. Each module is optimized individually for different channel environments, making it difficult to optimize them cooperatively. Thus, the communication blocks are usually analyzed independently [11–13]. However, the optimization of each module cannot represent the overall optimization of the whole system, and the design of the entire system does not consider possible interactions between sub-modules [14,15]. For example, separate designs for modulator and encoder are considered sub-optimal [16].

Recently, Deep Learning (DL) has emerged in the field of communication with applications in modulation recognition [17–20], channel estimation [21–23], and end-to-end learning [14,24–26]. The end-to-end architecture allows optimization of the communication system as a whole and is considered to have the potential to achieve global optimum [14]. In particular, the end-to-end structure has been extended to MIMO in conventional wireless communication systems [27–29], and MC systems [3,15,30].

In general, a typical end-to-end model can jointly optimize the transmitter and receiver in one signaling process to learn an efficient representation of the interfered signal. In [14], such a communication system is first proposed in the physical layer, where an autoencoder structure is used to learn transmitter and receiver with deep neural networks (DNN) representation. Traditional communication modules on the transmitter node, such as encoding and modulation, are replaced by one DNN, while modules on the receiver node, such as demodulation and decoding, are replaced by another. The autoencoder structure is trained offline using a Stochastic Gradient Descent (SGD) approach by optimizing the end-to-end loss function, which reflects recovery accuracy. Then, the gradients of transmitter can be back-propagated through the differentiable channel model, allowing the autoencoder to generate signals as close as possible to the transmitted ones. Thus, features and parameters of the end-to-end model can be learned directly from data instead of designing independent modules. In this paper, we consider the transmission, propagation, and reception of information molecules as an end-to-end MC system.

In end-to-end architectures, it is required that the underlying channel model is analytical, such as Additive White Gaussian Noise (AWGN) channel and Rayleigh fading channel. However, for MC, due to interference between signals and channels (**ISI and ILI**), environmental complexity, and other factors, various stochastic processes will be introduced, leading to non-differentiable channels. Thus, the back-propagation of gradients from receiver to transmitter is blocked, preventing the overall learning of the end-to-end system. The key of optimizing an end-to-end system is the accurate representation of channel information. To address unknown channels in end-to-end learning of communication systems, mathematical channel models can be estimated. However, it may not accurately reflect the actual transmission, leading to deviations from the real channel and thus degrading the overall system performance.

Recently, different DL-based **channel modeling** techniques have been proposed to address the problem of channel agnosticism, e.g., in [31], the modulation schemes for learning in two agents with a fully decentralized fashion are proposed to serve as a reinforcement learning problem, [32,33] are solved by designing the transmitter as a reinforcement learning agent, and in [34], a novel quantization is proposed for feedback signals which can communicate even with limited reward feedback.

Nevertheless, all the above schemes require a large amount of sample information from the receiver to the transmitter. Considering that generative adversarial networks (GANs) [35] are a powerful generative model that can be used to solve the problem of insufficient samples, it is used to simulate the channel [36]. By considering GAN as the substitution of the channel, the distribution of channel output can be learned directly from receiver observations, allowing transmitter gradients to be back-propagated. Specifically, generator in GAN generates fake received signals to approximate the distribution of the real received signals, and both real and fake signals are used to train the transmitter and receiver. In this way, the training of entire end-to-end system can be completed, and signal detection can be implemented. However, there are two drawbacks in original GAN, including the vanishing gradient caused by inappropriate loss functions and model collapse due to the loss of diversity caused by generator, making it incapable of achieving realistic channel models and intractable for GAN-based training schemes. Moreover, the end-to-end system cannot be well-trained if the sample size of real signals is too small.

To address these issues, evolutionary generative adversarial network (EGAN) [37] based on the idea of evolutionary computation is introduced. Evolutionary computation is inspired by biological evolution to solve complex optimization problems. It is expected that its optimization mechanism could solve the problem of vanishing gradient and model collapse. Here, the adversarial procedure in GAN is considered as an optimization issue in original EGAN, allowing generators to get solutions through evolutionary operators, including crossover, mutation, and selection, gradually obtaining suitable solutions in continuous iterations. One of the three mutations used in the original EGAN, least-squares mutation, causes over-punishment of fake samples and leads to training instability. Due to the fact that Kullback–Leibler divergence is a commonly used measurement of the similarity between two probability distributions and can better fit end-to-end systems, it is applied to improve the performance of the original EGAN.

In this paper, a channel-agnostic end-to-end learning method based on KLD EGAN is proposed for the newly developed MIMO MC with drift system, which can improve the transmission rate and obtain data for further training. In the end-to-end architecture, the channel representation, as well as the coding and decoding processes, are jointly optimized into a single end-to-end task. Specifically, the transmitter DNN replaces the coding and modulation module to achieve the release of molecules, and the receiver DNN replaces the demodulation and decoding module to perform signal detection. Moreover, channel KLD EGAN is used as a surrogate to enable the transmitter gradients back-propagate and to generate fake data for end-to-end training in case of insufficient sample size. By iteratively training the KLD EGAN, transmitter DNN, and receiver DNN, the entire system can automatically learn the channel output distribution and optimize the end-to-end loss without an explicit channel model.

To the best of our knowledge, the idea of integrating GAN and evolutionary computation is first introduced for end-to-end modeling in MIMO MC with drift system. As a data-driven approach, it provides new insight into the optimization of communication systems for a wide range of wireless channels. Unlike traditional signal processing algorithms which require channel information and thresholds, end-to-end learning can achieve signal detection through simple matrix operations. Moreover, the end-to-end architecture can approach or even exceed traditional systems in bit error rate (BER) performance with lower complexity, potentially achieving global optimum. The effectiveness and robustness of our model are demonstrated and analyzed.

The contributions of this paper are as follows:

1. We develop a mathematical MIMO MC with drift system paradigm to interpret the emission, propagation, and reception of information molecules. The additional drift term mitigates the effects of ISI, ILI, and other possible noise on the transmitted signal and thus decreases the transmission error.
2. With the consideration of KLD EGAN as a channel substitution, an end-to-end learning communication system is developed, which does not require an explicit channel model and can learn end-to-end links implicitly from data.
3. Compared with other DL-based methods, including DNN, original GAN, and original EGAN, the proposed KLD EGAN has the capability of addressing the issues of vanishing gradient and model collapse in GAN, and over-punishment in EGAN, respectively, thus generating more realistic signals. The system can still be trained effectively with the generated fake signals, even with only a small training sample size.

2. System model

In this work, MC system with W **point transmitters,** W **spherical passive receivers**, and a diffusion-based channel with drift in a three-dimensional (3D) environment is considered. The transmitter can instantaneously release a predefined number of information molecules simultaneously, which would then propagate along the fluid medium by both the Brownian motion and the drift. It is assumed that interactions and elastic collisions between information molecules are not taken into account when there are multiple information molecules in the environment. Here, all the molecules have the same properties in terms of shape and size. Furthermore, the transmitters and receivers are considered to be synchronized.

During the entire communication process, there exist two kinds of interference which would affect the reception of information molecules at the receiver. Firstly, due to the low-speed characteristic of diffusion and uncertainty of molecular Brownian motion, the receiver may receive molecules emitted from all previous time slots by the transmitter at current time slot, resulting in ISI. In addition, the transmitter is assumed to transmit independent signals to its corresponding receiver. Given that all transceiver links use the same molecules for transmission, the receiver may receive molecules sent by the non-corresponding transmitter, resulting in ILI.

2.1. Topology and propagation model

A $W \times W$ MIMO system is shown in Fig. 1. The transmitters are denoted as Tx1, Tx2, …, TxW, while the receivers are denoted as Rx1, Rx2, …, RxW. Each transmitter is located at a distance d from the center of its corresponding spherical receiver. All receivers have the same radius r and are separated by a distance h, same as the distance between each transmitter.

The transmitter encodes the signal by the concentration of information molecules, which are released, propagate through the channel by Brownian motion and drift, and are finally observed by the receiver. Thus, the receiver decodes the signal according to the number of arrived molecules. The transmission time is divided into time slots of equal duration t_s. Here, the binary concentration shift keying (BCSK) modulation scheme is applied, where the release of a predefined number of molecules in t_s is represented by binary 1, and no release is 0. Only one bit is transmitted in each time slot t_s. For the wth transmitter and receiver, the coordinates under 3D Cartesian coordinate system are set as follows: $\mathbf{d}_{\mathrm{Tx}w} = [0, 0, (w-1)h]$ for Txw, $\mathbf{d}_{\mathrm{Rx}w} = [d, 0, (w-1)h]$ for the center of Rxw, and $\mathbf{d}(t) = [x_t, y_t, z_t]$ for the position of information molecule at time t.

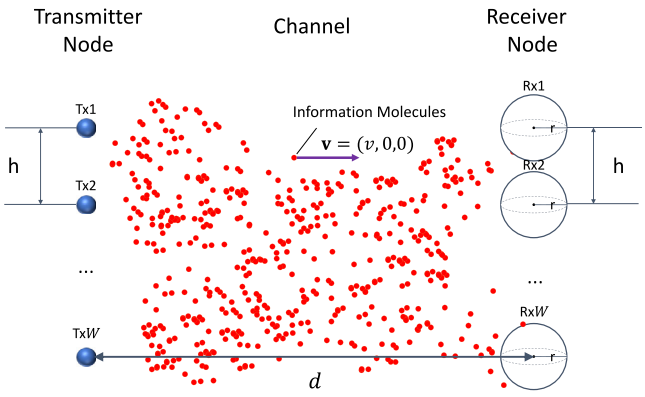

Fig. 1. Schematic of proposed MIMO MC with drift system.

To demonstrate the proposed model, we use Rx1 Receiver as an example to illustrate the propagation of molecules. Other receiver models are similar to the Rx1. In general, the effect of advection can be described by a velocity vector $\mathbf{v}(\mathbf{d}, t)$ depending on position $\mathbf{d}$ and time t. Here, a constant uniform flow along the positive x-axis is considered. Also, let $c(\mathbf{d}, t)$ denote the concentration of molecules, i.e., the average number of molecules at coordinates $\mathbf{d}$ and time t. Since the molecules are affected by both free diffusion and drift, the propagation process of molecules can be characterized by the advection–diffusion equation in (1) [38].

$$\frac{\partial c(\mathbf{d}, t)}{\partial t} = D_c \nabla^2 c(\mathbf{d}, t) - \nabla \cdot (\mathbf{v}(\mathbf{d}, t) c(\mathbf{d}, t)), \tag{1}$$

where ∇^2 and ∇ are the Laplace operator and the Hamiltonian in Cartesian coordinate, respectively, and D_c is the diffusion coefficient. Moreover, considering an unbounded 3D environment with impulse response, initial conditions (IC) and boundary condition (BC) are represented as follows [38]:

$$\begin{cases} \mathrm{IC} : c\left(\mathbf{d}_{\mathrm{Tx}w}, t \to 0\right) = \delta\left(\mathbf{d} - \mathbf{d}_{\mathrm{Tx}w}\right), \\ \mathrm{BC} : c(\|\mathbf{d}\| \to \infty, t) = 0, \end{cases} \tag{2}$$

where $\delta(\cdot)$ is the Dirac delta function.

By solving (1) with IC and BC, the probability of observing one molecule per unit volume, which is consistent with the definition of probability density function (PDF) with respect to position $\boldsymbol{d}$ at time t, can be expressed as [38]:

$$f(\mathbf{d}, t) = \frac{1}{(4\pi D_c t)^{3/2}} \cdot \exp\left(-\frac{\|\mathbf{d} - t\mathbf{v} - \mathbf{d}_{\mathrm{Tx}w}\|^2}{4 D_c t}\right). \tag{3}$$

By integrating PDF in the x, y, z direction, we can obtain the probability of observing a single molecule, denoted as $f(\mathbf{d}, t)\, dxdydz$, in a rectangular cube of length dx, height dy, and depth dz, centered on $\mathbf{d}$ at time t. According to the Uniform Concentration Assumption (UCA) [38], when the receiver is placed far away from the transmitter, PDF for all points within the receiver volume can be approximated to the value at the center of receiver. In this way, the probability of capturing a molecule observed at receiver can be derived as (4) by integrating the receiver volume:

$$P(\mathbf{d}, t) = \frac{V_r}{(4\pi D_c t)^{3/2}} \cdot \exp\left(-\frac{\|\mathbf{d} - t\mathbf{v} - \mathbf{d}_{\mathrm{Tx}w}\|^2}{4 D_c t}\right), \tag{4}$$

where V_r is the volume of spherical receiver. By applying $\mathbf{d}_{\mathrm{Tx}w}$ and $\mathbf{d}_{\mathrm{Rx}1}$ to (4), the probability of observing one molecule by wth paired and unpaired transceiver can be written as (5) and (6), respectively.

$$P_{pair}(t) = \frac{V_r}{(4\pi D_c t)^{3/2}} \cdot \exp\left(-\frac{(d - tv)^2}{4 D_c t}\right), \tag{5}$$

$$P_{unpair_w}(t) = \frac{V_r}{(4\pi D_c t)^{3/2}} \cdot \exp\left(-\frac{(d - tv)^2 + ((w-1)h)^2}{4D_c t}\right), \quad (6)$$

where v is the drift velocity.

It is assumed that n information molecules are emitted by Tx1 at the start of each time slot. Since each molecule is transmitted independently, the number of molecules observed by the receiver, denoted as N, follows a binomial distribution. Furthermore, when n is sufficiently large, the binomial distribution can be approximated as a normal distribution. Thus, we can obtain the distribution of the number of molecules received by Rxw as (7) and (8) for $w = 1$ and $1 < w \leq W$, respectively.

$$N_{pair}(n, t) \sim \mathcal{B}(n, P_{pair}(t)) \sim \mathcal{N}(nP_{pair}(t), nP_{pair}(t)(1 - P_{pair}(t))), \quad (7)$$

$$N_{unpair_w}(n, t) \sim \mathcal{B}(n, P_{unpair_w}(t)) \sim \mathcal{N}(nP_{unpair_w}(t), nP_{unpair_w}(t)(1 - P_{unpair_w}(t))). \quad (8)$$

In this MIMO communication system, interferences come from three aspects, specifically from ISI, ILI, and possible channel Gaussian noise originating from molecular decomposition or other nano-machine emissions, denoted as $N_{noise} \sim \mathcal{N}(0, \sigma_n^2)$. Both ISI and ILI can lead to that the symbols received in the current time slot are not all sent by the paired transmitter in the same time slot, resulting in signal distortion and thus affecting signal detection. In particular, only the previous one time slot is considered in this paper for simplicity.

It is assumed that the transmitters have independent sequences of $\boldsymbol{s}_w$ as their respective signals, which are to be sent to the corresponding receivers Rxw. All the transmitted sequences are concatenated to achieve the original transmitted signal $\boldsymbol{s} = [\boldsymbol{s}_1, \boldsymbol{s}_2, \ldots, \boldsymbol{s}_W]^T$. Therefore, the number of molecules observed by the receiver Rx1 at the jth time slot can be expressed as

$$N(j, t) = s[1]N_{pair}(n, t) + \underbrace{\sum_{i=1}^{m} s_1[j-i]N_{pair}(n, t + it_s)}_{ISI} + \underbrace{\sum_{i=0}^{m}\sum_{w=2}^{W} s_w[j-i]N_{unpair_w}(n, t + it_s)}_{ILI} + N_{noise}(j), \quad (9)$$

where m is the length of channel memory, which is set to 1 in this paper. In this equation, ISI term considers only the effect of the previous time slot from the paired transmitter, while ILI term considers the effect of both the current and previous time slots from the unpaired transmitter.

In this work, the number of information molecules observed at the receiver node is considered to be the observation signal and is used to decode the transmitted signal. Since the transceivers are assumed to be synchronous, each transmitted symbol corresponds to an individual observation symbol. Thus, the observation signals $\boldsymbol{y}$ for each time slot of Rx1 is expressed as (10):

$$\boldsymbol{y} = \begin{bmatrix} N(1, t) \\ N(2, t) \\ \vdots \\ N(\frac{I}{W}, t) \end{bmatrix} = \begin{bmatrix} H_1 \mid \ldots \mid H_W \end{bmatrix} \begin{bmatrix} s_1[1] \\ \vdots \\ s_1[\frac{I}{W}] \\ \vdots \\ s_W[1] \\ \vdots \\ s_W[\frac{I}{W}] \end{bmatrix}, \quad (10)$$

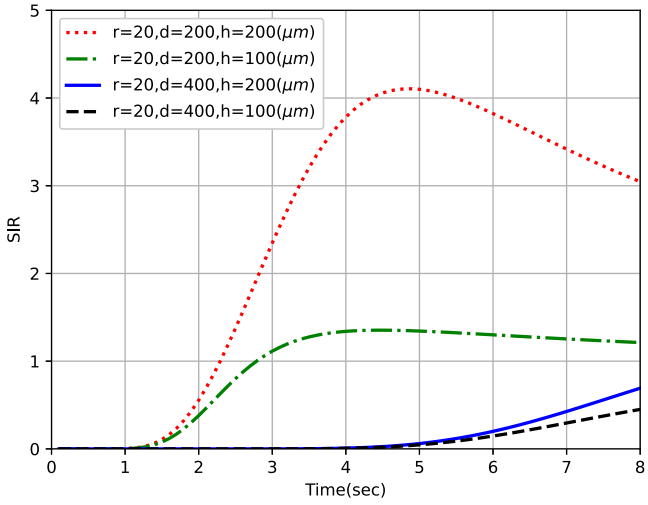

Fig. 2. SIR on different topology parameters.

where

$$H_1 = \begin{bmatrix} N_{pair}(n, t) & & \\ N_{pair}(n, t + t_s) & N_{pair}(n, t) & \\ & \cdots & \cdots \\ & & N_{pair}(n, t + t_s) \;\; N_{pair}(n, t) \end{bmatrix}_{\frac{I}{W} \times \frac{I}{W}},$$

$$H_w = \begin{bmatrix} N_{unpair_w}(n, t) & & \\ N_{unpair_w}(n, t + t_s) & N_{unpair_w}(n, t) & \\ & \cdots & \cdots \\ & & N_{unpair_w}(n, t + t_s) \;\; N_{unpair_w}(n, t) \end{bmatrix}_{\frac{I}{W} \times \frac{I}{W}}.$$

where I is the length of transmitted sequence, which is divided into W portions for transmission.

2.2. Signal-to-interference ratio

To quantify the effect of different system topological parameters and drift velocities on the number of arrived molecules, the signal-to-interference ratio (SIR) is defined. The SIR represents the ratio of molecules received from the paired transmitter in the current time slot to the average number of molecules from all ISI, ILI, and Gaussian noise parts, which is expressed as (11) at the jth time slot. Obviously, a higher SIR value indicates a higher performance of the MIMO communication system (see Box I).

For simplicity, we set $W = 2$. Fig. 2 shows the SIR values for different topology parameters. Both increasing d and decreasing h cause the degradation of SIR because the former increases ISI and the latter increases ILI. Moreover, it can be observed that the parameter d has a more significant effect on the system, and thus ISI has a stronger impact on SIR compared with ILI. t_s is set as 8(s) in this work.

Fig. 3 shows the SIR values for different drift velocities. By increasing the drift velocity v, both ISI and ILI can be alleviated to some extent, reducing the randomness of molecular motion and thus obtaining a higher SIR value.

2.3. Particle-based simulation

To validate the accuracy of the mathematical model proposed in Section 2.1, we record the position of each molecule at each

$$\mathrm{SIR} = \frac{s[j]N_{pair}}{\left(\sum_{i=1}^{m} s_1[j-i]N_{pair}\,(n, t+it_s) + \sum_{i=0}^{m}\sum_{w=2}^{W} s_w[j-i]N_{unpair_w}\,(n, t+it_s) + N_{noise}(j,t)\right)/3}. \tag{11}$$

Box I.

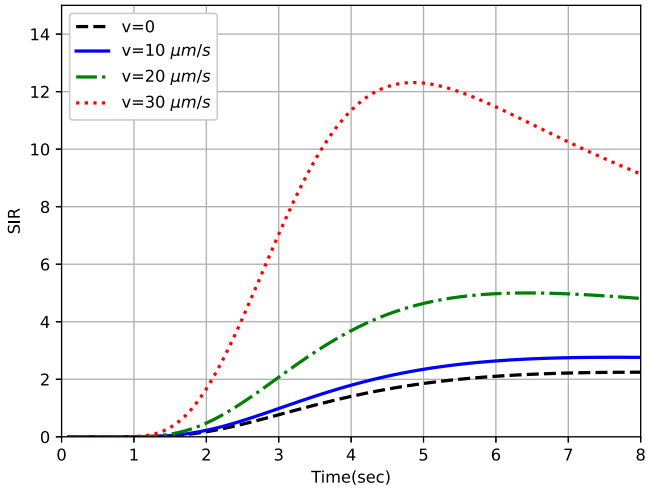

Fig. 3. SIR on different drift velocity.

moment using the particle-based simulation, which is represented as:

$$\begin{aligned}(x_t, y_t, z_t) &= (x_{t-\Delta t}, y_{t-\Delta t}, z_{t-\Delta t}) + (\Delta x, \Delta y, \Delta z),\\ \Delta x &\sim \mathcal{N}(v\Delta t, 2D_c\Delta t),\\ \Delta y &\sim \mathcal{N}(0, 2D_c\Delta t),\\ \Delta z &\sim \mathcal{N}(0, 2D_c\Delta t),\end{aligned} \tag{12}$$

where x_t, y_t, z_t are the molecules' positions at each dimension at time t.

We set $W = 2$. It is assumed that the signal to be transmitted is [1, 0, 0, 1, 1, 0, 1, 0, 1, 0]. Tx1 transmits [1, 0, 0, 1, 1] and Tx2 transmits [0, 1, 0, 1, 0]. The number of molecules observed by Rx1 is shown in Fig. 4. The total number of molecules entering spherical receiver in one simulation is recorded as a single simulation, and this process is repeated ten times and averaged as the average simulation. The theoretical curve is obtained using (5) and (6), where the system parameters are shown in Table 1. The parameters are chosen by selecting the best set discussed in Section 2.2. As shown in Fig. 4, theoretical values can be well-fitted to the average simulation values, proving that the proposed model can perfectly represent the molecular propagation process in the channel.

3. DL-based end-to-end paradigm

In this section, we illustrate how to decode the transmitted signals using DL-based methods, specifically GAN-based, KLD EGAN-based, and DNN-based methods, which are subsequently evaluated through BER performance. In original GAN, original EGAN, and KLD EGAN-based models, the underlying channel is unknown, and we only use the data sampled from the theoretical MIMO MC system with drift proposed in Section 2 in the offline training phase. However, in DNN-based model, analytical representation of the underlying channel is supposed to be known.

Table 1
The Default Parameters of Molecular Communication System.

Parameters	Value
Transceiver number(W[a])	2
Radius of the receiver (r)	20 μm
Height (h)	200 μm
Distance (d)	200 μm
Diffusion coefficient (D_c[a])	800 $\mu m^2/s$
Drift velocity (v[a])	30 μm/s
Molecules per bit (n[a])	30000

[a]Parameters that may change during experiments.

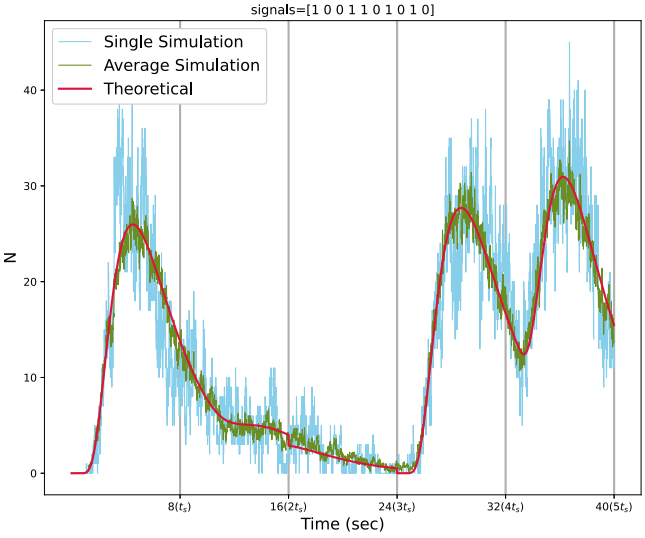

Fig. 4. Particle-based simulation results of Rx1 for distance $d = 20$ μm, height $h = 200$ μm, radius $r = 20$ μm, drift velocity $v = 30$ μm/s.

3.1. End-to-end learning for MIMO system

Due to the topology of proposed system, the properties of different paired transceivers are similar. Therefore, their respective original signals can be concatenated to train the end-to-end system. Fig. 5(a) depicts the end-to-end architecture of the communication system. The parameters of transmitter DNN and receiver DNN are represented by θ_{Tx} and θ_{Rx}, respectively. The signal transmitted by Txw is denoted as $\boldsymbol{s_w}$, taken from the alphabet $\mathcal{M} = \{0, 1\}$. All the $\boldsymbol{s_w}$ are concatenated as $\boldsymbol{s}$, which has been stated. Next, $\boldsymbol{s}$ is mapped to a one-hot vector, with 0 denoted as $[1, 0]^T$ and 1 denoted as $[0, 1]^T$. The dimension of $\boldsymbol{s}$ is $W \times \frac{I}{W} \times 2$, which is then modulated as $\boldsymbol{x} = f_{\theta_{\mathrm{Tx}}}(\boldsymbol{s}), \boldsymbol{x} \in \mathbb{R}^{\{3\}}$. The channel takes $\boldsymbol{x}$ as input such that its output $\boldsymbol{y}$ follows the conditional probability distribution $\boldsymbol{y} \sim p(\boldsymbol{y}|\boldsymbol{x})$. Correspondingly, the receiver decodes the received channel output $\boldsymbol{y}$ to a probability vector $\mathbf{p}$ represented as $\mathbf{p} = f_{\theta_{\mathrm{Rx}}}(\boldsymbol{y})$, where the sum value of the lowest dimension of $\mathbf{p}$ is 1. Eventually, the receiver takes the dimension of the maximum value of $\mathbf{p}$ as the decoded signal

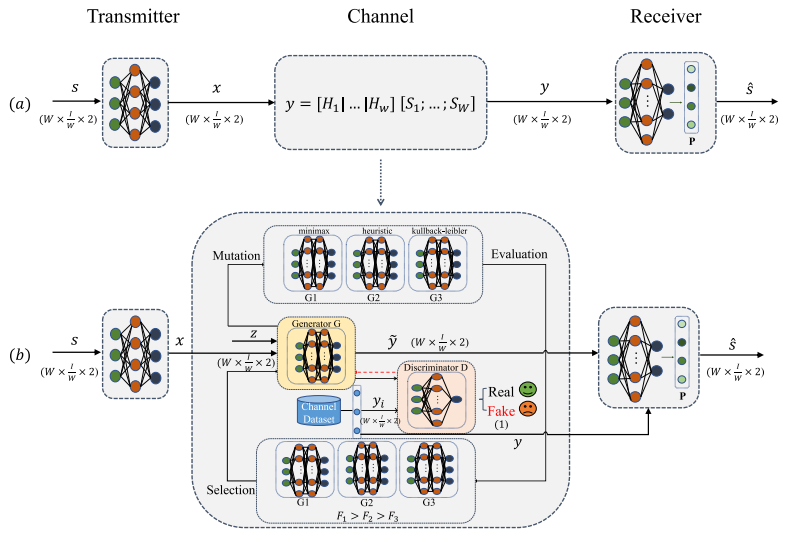

Fig. 5. End-to-end learning based communication systems: (a) end-to-end communication system, where transceiver is represented by neural networks; (b) proposed end-to-end communication system, where channel is represented by KLD EGAN.

$\hat{\boldsymbol{s}} = \arg\max_{\boldsymbol{s}}(f_{\theta_{\mathrm{Rx}}}(\boldsymbol{y}|f_{\theta_{\mathrm{Tx}}}(\boldsymbol{s})))$. The end-to-end MC system aims to achieve a better signal recovery capability.

To minimize the difference between transmitted signal $\boldsymbol{s}$ and recovered signal $\hat{\boldsymbol{s}}$, the distance is measured using the binary cross-entropy end-to-end loss, which can be expressed as:

$$\mathcal{L} = \sum_{j=1}^{I}(s[j]\log(\hat{s}[j]) + (1 - s[j])\log(1 - \hat{s}[j])), \tag{13}$$

where $s[j]$ and $\hat{s}[j]$ represent the jth element of $\boldsymbol{s}$ and $\hat{\boldsymbol{s}}$, respectively, and I is the length of transmitted sequence.

3.2. GAN-based model for MIMO system

3.2.1. Generative adversarial network

GAN [35] is a typical framework for estimating generative models through an adversarial process with two components: generator G and discriminator D, which are implemented by neural networks with trainable parameters θ_{G} and D, respectively. The training objective of G is to generate data similar to the real data as much as possible and to adjust its parameters to eliminate the difference between the two data distributions and fool D. The training objective of the D is to determine, as far as possible, whether the samples fed into D are real or not. The whole process can be considered as a two-player minimax game between D and G [35]. Under the determination of D, G gradually learns the real data distribution by adjusting θ_{G}. The random noise z is used as an input to G, and the fake samples $G(z)$ are the output. As for D, the input includes both the real samples a from the dataset and the fake samples $G(z)$. The output of D is a probability value to determine whether the input samples are true or fake. θ_{G} and θ_{D} are independent of each other, and the adversarial training procedure could be represented by:

$$\min_{G}\max_{D} V(D, G) = \mathbb{E}_{a\sim p_{data(a)}}[\log D(a)] + \mathbb{E}_{z\sim p_z}[\log(1 - D(G(z)))], \tag{14}$$

where $p_{data(a)}$, p_z are the probability distribution functions of the real sample a, and the input noise z, respectively.

Since G and D are trained alternately during the entire procedure, (14) could be divided into two parts. The training objective for G and D can be respectively represented by:

$$\min_{G} V(D, G) = \mathbb{E}_{z\sim p_z}[\log(1 - D(G(z)))], \tag{15}$$

$$\max_{D} V(D, G) = \mathbb{E}_{a\sim p_{data(a)}}[\log D(a)] + \mathbb{E}_{z\sim p_z}[\log(1 - D(G(z)))]. \tag{16}$$

3.2.2. GAN-based training scheme

In the GAN-based end-to-end architecture, both the transmitter and receiver are replaced by DNN, and the channel is substituted with channel GAN. The transmitter and receiver are trained to minimize the end-to-end loss represented by (13). The generator G and discriminator D are trained by (15) and (16), respectively, where the real data for D is sampled from the MIMO MC with drift system. Channel GAN simulates the output distribution of the real channel as much as possible in adversarial training and feeds the generated fake signals together with the real sampled signals to the receiver for decoding. In addition, the gradients of transmitter can be back-propagated through G to complete the end-to-end training of the whole architecture.

3.3. KLD EGAN-based model for MIMO system

3.3.1. Evolutionary generative adversarial network

According to [35], if the discriminator achieves optimum in original GAN stated above, the minimax objective function (14) aims to minimize the Jensen–Shannon divergence (JSD) between real and generated distributions. However, if the overlap between real and generated distributions is pretty tiny in the early training stage, i.e., the quality of generated samples is less than satisfactory, JSD will be a constant, causing vanishing gradient [37]. Evolutionary computation, which is based on concepts of biological evolution, has the potential to address the above issue. In evolutionary computation, a population of possible solutions to the target problem is first created, each of which is considered as an individual in the population. With the operators such as mutation and crossover, individuals would produce new solutions based on the initial population. Each newly generated individual is considered as an offspring and each offspring is measured by a fitness function which indicates its quality. Offspring with better fitness values are selected for the next evolutionary process. The population evolves over time until reaching a predefined condition and gradually finds better solutions [39].

EGAN is first proposed in [37]. In each evolutionary process, EGAN evolves a population of individuals, and each individual

(served as the generator G) represents a potential solution in the solution space. The environment (served as the discriminator D) provides different fitness loss functions which would guide the individual in evolving under different mutations. Thus the population gradually adapts to the environment, indicating that more realistic data would be produced. During each evolutionary process, there exist three sub-stages.

1. **Mutation:** Mutation is the variation of individual genes under the influence of the environment, which may introduce new information into offspring and explore the solution space not currently covered. In EGAN, there are three types of mutations, specifically minimax mutation, heuristic mutation, and least-squares mutation. In particular, minimax mutation corresponds to the minimax objective function in the original GAN.
2. **Evaluation:** A fitness function is used to measure the quality of each mutated offspring. Here, both the quality and diversity of the generated samples are used to determine the direction of evolution. The quality fitness function could be derived as follows. If the generated samples are realistic enough, they will be able to fool D and get a higher quality score.

$$\mathcal{F}_q = \mathbb{E}_z[D(G(z))]. \tag{17}$$

   In addition, the diversity of samples is also considered to mitigate the mode collapse issue. A smaller gradient value corresponds to more discrete generation samples, indicating a higher diversity. The diversity fitness function is given by (18), which is measured by using the log gradient value of updating D.

$$\mathcal{F}_d = -\log \|\nabla_D - \mathbb{E}_x[\log D(x)] - \mathbb{E}_z[\log(1 - D(G(z)))]\|. \tag{18}$$

   Thus, the fitness function can be modified as: $\mathcal{F} = \mathcal{F}_q + \gamma\mathcal{F}_d$, where γ is a weight parameter that balances the weight of sample quality and diversity.
3. **Selection:** Selection indicates the survival of the fittest, and this step simulates the process of natural selection. The offspring with better fitness values represents a better adaptation to the environment and will be selected for the following evolutionary process to find the optimal solution in the solution space.

3.3.2. KLD EGAN

In the least-squares mutation of original EGAN, we minimize the squared error between the real channel output value and the faked output value of G, with the expectation that the squared error between the two is minimized. However, least-squares mutation may cause an over-punishment of the fake samples and is strongly influenced by outlier perturbations [40]. Kullback–Leibler divergence (KLD) is widely used to measure the difference between two distributions, specifically, it describes the coding loss of using the distribution simulated by G to estimate the true distribution of channel output signal. Moreover, sufficient gradients can be consistently provided throughout the entire training process, thus Kullback–Leibler mutation is used for replacement in the channel model in this work.

By minimizing the loss of KLD, the amount of information loss is reduced as much as possible when replacing the real distribution with the one generated by G. In this way, the simulated distribution of G is almost identical to the real distribution, making it possible to train the end-to-end system better without the training instability caused by least-squares mutation. All three sub-stages, i.e., mutation, evaluation, and selection, are used for each training iteration. Both evaluation and selection phases of KLD EGAN are consistent with EGAN mentioned in Section 3.3.1. Three different mutation operators are as follows.

1. *Minimax mutation:*

$$\mathcal{M}^{\text{minimax}} = \mathbb{E}_{z\sim p_z}[\log(1 - D(G(z)))], \tag{19}$$

2. *Heuristic mutation:*

$$\mathcal{M}^{\text{heuristic}} = -\mathbb{E}_{z\sim p_z}[\log(D(G(z)))], \tag{20}$$

3. *Kullback–Leibler mutation:*

$$\mathcal{M}^{\text{kullback-leibler}} = \mathbb{E}_{z\sim p_z} D(G(z))[\log(D(G(z)) - 1)]. \tag{21}$$

These different mutation operators correspond to different training objectives. For example, given an individual G in the population, three mutation operators are utilized to generate its offspring {G1, G2, G3}. Specifically, three copies of each individual are created, each of which are modified by different mutations. Then, each modified copy is considered as one offspring. Different mutation operators attempt to reduce the distances between the generated distribution and the data distribution from different perspectives [37]. For each evolutionary process, the generator is updated with three objectives (or mutations) to accommodate the current environment. If one mutation strategy could not provide sufficient gradient, another is applied in the next iteration. According to the principle of "survival of the fittest", only the best-performing offspring will survive and participate in future training. In addition, both the sample quality and sample diversity are taken into account for evaluation.

3.3.3. KLD EGAN-based training scheme

In the KLD EGAN-based end-to-end architecture, transmitters and receivers are replaced with DNN, and the channel is substituted with channel KLD EGAN. Since the end-to-end loss is calculated at the receiver, it is easy to obtain its gradients and to train the receiver parameters θ_{Rx}. When updating the transmitter parameters θ_{Tx}, channel KLD EGAN is used as the surrogate channel so the gradients can be back-propagated. In addition, as shown in Fig. 5(b), both real sampled data and fake data generated by G are fed into the receiver for training. Thus, the effectiveness of the end-to-end system can be guaranteed even with insufficient training samples. Also, with a more realistic channel output generated by G, better training of the communication system can be achieved, allowing the receiver to decode and recover the original transmitted signal more accurately.

The training details of channel KLD EGAN are illustrated in Algorithm 1. In each iteration, D is first updated. By sampling a batch of transmitted signal $\boldsymbol{s}$, the encoded information $\boldsymbol{x}$ can be obtained from the output of the transmitter. In addition, the random noise $\boldsymbol{z}$ needs to be sampled. The real data can be obtained from the MIMO MC with drift system in Section 2, and the fake data can be obtained from G. Both of them are fed into D. Identical to D, a batch of $\boldsymbol{s}$ and $\boldsymbol{z}$ need to be sampled when updating G. For each evolutionary iteration, G is updated with different mutations to accommodate the current environment, where the number of mutations is denoted as n_m. After evaluating all offspring, the optimal one is selected for the next iteration.

3.4. DNN-based model for MIMO system

DNNs are neural networks with a number of hidden layers. In DNN-based model, the network architecture of transmitter and receiver remains the same as in GAN-based and KLD EGAN-based approaches. Fig. 5(a) shows the structure of DNN-based model. Two differences are that the underlying channel for DNN-based architecture is known, and only the real signals are sampled to

Algorithm 1: Channel KLD EGAN Training Algorithm.

Require: Initialization:N_{train}; γ; n_m; $BatchSize(bs)$;
Require: Initialize θ_{Tx},θ_{Rx},θ_{G},θ_{D}; Generate N_{train} training data samples at random;
for number of training iterations **do**
  % Updating the Discriminator
  Sample a batch of transmitted data for Tx $\{s^b\}_{b=1}^{bs}$.
  Sample a batch of noise $\{z^b\}_{b=1}^{bs}$.
  Get the transmitted information $\{\boldsymbol{x}\} \leftarrow f_{\theta_{\mathrm{Tx}}}(\boldsymbol{s})$.
  Get the channel output signal $\{\boldsymbol{y}\} \leftarrow f_{\theta_{\mathrm{G}}}(\boldsymbol{x}, \boldsymbol{z})$.
  Derive the received signal $\{\hat{\boldsymbol{s}}\} \leftarrow f_{\theta_{\mathrm{Rx}}}(\boldsymbol{y})$.
  Sample a batch of real channel signal from MIMO MC with drift system.
  Update the discriminator by SGD($\nabla_{\theta_{\mathrm{D}}}[\frac{1}{bc}\sum_{b=1}^{bs} logD_{\theta_{\mathrm{D}}}(x^b)+\frac{1}{bc}\sum_{b=1}^{bc} log(1-D_{\theta_{\mathrm{D}}}(G_{\theta_{\mathrm{G}}}(z^b))]$).
  % Updating the Generator
  Sample a batch of transmitted data $\{s^b\}_{b=1}^{bs}$.
  Sample a batch of noise $\{z^b\}_{b=1}^{bs}$.
  for $j = 1, ..., n_m$ **do**
    Mutate individual $G_{\theta_{\mathrm{G}}^j} \leftarrow \nabla\mathcal{M}_{\mathrm{G}}^j(\{z^b\}_{b=1}^{bs})$.
    Sort the mutated individual $\mathcal{F}^j \leftarrow \mathcal{F}_q^j + \gamma\mathcal{F}_d^j$.
  end for
  Select the optimal one to be the next generator $\{\mathcal{F}^{j_1}, \mathcal{F}^{j_2}, ...\} \leftarrow sort(\mathcal{F}^j)$.
  $G_{\theta_{\mathrm{G}}} \leftarrow G_{\theta_{\mathrm{G}}{}^{j_{best}}}$
end for

train the system. The end-to-end loss defined in (13) is minimized by decoding signals at the receiver according to the channel output. The gradients of receiver DNN are then obtained, while the gradients of transmitter DNN can be back-propagated through the differentiable channel model to complete the end-to-end training.

4. Traditional detection algorithms

In this paper, our proposed method is compared with two traditional detection algorithms to analyze BER performance. Note that both maximum a posterior (MAP) detector and fixed threshold (FT) detector require the underlying channel model to be known when recovering the original signal sent by the transmitter at the receiver node, which is different from our proposed data-driven approach.

4.1. MAP detector

The MAP detector traverses all possible transmission sequences and takes the sequence that maximizes the posteriori probability density function (PDF) of the received signal as a result. Since the MAP detector incorporates the prior distribution of the quantity to be estimated in it, it is considered to be the optimal detector to achieve theoretical BER performance. Thus, MAP detector determines the sequence of transmitted bits by maximizing the joint PDF of the transmitted bits $\boldsymbol{s}$ and the observation signals $\boldsymbol{y}$, which is expressed as (22)[41]:

$$\hat{\boldsymbol{s}} = \arg\max_{\boldsymbol{s}} \prod_{j=0}^{\frac{l}{W}} f_h\left(y[j] \mid \boldsymbol{s}[j-1, j]\right). \tag{22}$$

where f_h is the joint PDF of observed signal samples $\boldsymbol{y}$ and transmitted signal $\boldsymbol{s}$.

For decoding the jth bit of $\boldsymbol{s}$ sequences, we calculate the probability of a normal distribution where the jth bit is 0 or 1 based on the result of $(j-1)$th bit, followed by traversing all cases to find the maximum value as the result.

4.2. Fixed threshold detector

Inspired by practical zero forcing method proposed in [42], we proposed the fixed threshold (FT) detector in this paper. The distribution of the observed signals is different for sending bits 0 and 1. And two fixed thresholds for signal decoding can be obtained by finding the intersection of these two distributions.

Assuming that bits 0 and 1 are emitted with identical probability, the mean and the variance of total interference, i.e., ISI and ILI, are expressed as :

$$\mu_I = \frac{1}{2}n\left(P_{pair}(2t_s) + \sum_{w=2}^{W}(P_{unpair_w}(t_s) + P_{unpair_w}(2t_s))\right), \tag{23}$$

$$\begin{aligned}\sigma_I^2 = (\frac{n}{2})^2\Big[(P_{pair}(2t_s))^2 + \sum_{w=2}^{W}(P_{unpair_w}(t_s))^2 + \sum_{w=2}^{W}(P_{unpair_w}(2t_s))^2\Big] \\ + \frac{n}{2}\Big[P_{pair}(2t_s)(1-P_{pair}(2t_s)) + \sum_{w=2}^{W}(P_{unpair_w}(t_s)(1-P_{unpair_w}(t_s))) \\ + \sum_{w=2}^{W}(P_{unpair_w}(2t_s)(1-P_{unpair_w}(2t_s)))\Big],\end{aligned} \tag{24}$$

where $P_{pair}(2t_s)$ is the probability of a molecule arriving at the corresponding receiver in next time slot. $P_{unpair_w}(t_s)$ and $P_{unpair_w}(2t_s)$ are the probability of a molecule arriving at the non-corresponding receiver Rxw in current time slot and in the next time slot, respectively.

Furthermore, the probability density function of $\boldsymbol{y}_{FT}$ when transmitting 0 and 1 bits, denoted as $\boldsymbol{y}_{FT|0}$ and $\boldsymbol{y}_{FT|1}$, respectively, can be represented as follows.

$$\begin{cases}\boldsymbol{y}_{FT|0} \sim \mathcal{N}\left(\mu_0, \sigma_0^2\right) = \mathcal{N}\left(\mu_I, \sigma_I^2 + \sigma_n^2\right), \\ \boldsymbol{y}_{FT|1} \sim \mathcal{N}\left(\mu_1, \sigma_1^2\right) = \mathcal{N}\left(\alpha + \mu_I, \alpha(1-P_{pair}(t_s)) + \sigma_0^2\right),\end{cases} \tag{25}$$

for $\alpha = n \times P_{pair}(t_s)$.

The intersection of these two distributions is the decoding threshold η. Within this threshold, the symbol is decoded as 0, otherwise, it is decoded as 1. Let

$$\frac{1}{\sigma_0\sqrt{2\pi}}\exp\left(-\frac{(\eta-\mu_0)^2}{2\sigma_0^2}\right) = \frac{1}{\sigma_1\sqrt{2\pi}}\exp\left(-\frac{(\eta-\mu_1)^2}{2\sigma_1^2}\right), \tag{26}$$

we can obtain the threshold as:

$$\eta = \mu_0 + \frac{-\alpha \pm \sqrt{\alpha^2 + (\beta^2-1)\left(\alpha^2 + \sigma_0^2\beta^2\ln\beta^2\right)}}{\beta^2-1}, \tag{27}$$

for $\beta = \sigma_1/\sigma_0$. Once the threshold is obtained, the decoding process can be defined as:

$$\hat{\boldsymbol{s}} = \delta\left(\hat{\boldsymbol{y}}_{FT}\right) = \begin{cases} 0 & \eta_s < \hat{\boldsymbol{y}}_{FT} < \eta_b \\ 1 & \text{otherwise}\end{cases} \tag{28}$$

where η_s and η_b are the smaller threshold and bigger threshold, respectively, and $\delta(\cdot)$ is the decoding function.

In FT detector, it is assumed that the decoded signal has the same number of 0 bits and 1 bits in pre-sequence signals. However, the assumption deviates from the actual situation. Moreover, in MAP detector, the effect of actual pre-sequence signals is considered, leading to that the FT detector can only be considered as a sub-optimal detector.

Table 2
The Parameters of KLD EGAN-based End-to-end System.

Parameters	Value
Weight Parameter (γ)	0.05
Mutation Operator (n_m)	3
Batch Size (bs)	64
Transmitter: Neurons in one hidden layer	4
Learning rate	0.0001
Receiver: Neurons in one hidden layer	8
Learning rate	0.0001
Generator: Neurons in each hidden layers	16,16
Learning rate	0.0005
Discriminator: Neurons in one hidden layer	16
Learning rate	0.0005

5. Experiments and numerical results

In this section, a series of experiments with different parameters are carried out to evaluate the performance of proposed KLD EGAN-based model presented in Section 3.3 as well as others. MAP detector described in Section 4.1 and FT detector given in Section 4.2 is considered as the optimum and sub-optimum operator, respectively.

Assume that there are two pairs of transceivers, i.e., $W = 2$. As stated in Section 2.2, we have compared the SIR values of MIMO MC system under different topology parameters and selected the best to chose as the experimental conditions for this section. Specifically, the parameters are set as $d = \mathbf{200}$ μm, $h = 200$ μm, $r = 20$ μm, $v = 30$ μm/s. More specific experimental setup is given in Section 5.1. In Section 5.2, the generation capabilities of different GAN-based models, including original GAN, original EGAN, and KLD EGAN, are analyzed. In Section 5.4, the BER performance of various detectors for different model parameters, including the signal-to-noise ratios (SNR), number of molecules per bit, diffusion coefficient, drift velocity, and training sample size are evaluated.

5.1. Experimental setup

Fully connected (FC) layers are used for all neural networks in transmitter, receiver, and channel KLD EGAN. The weights of all models are updated by stochastic gradient descent (SGD) algorithm. The size of training data and testing data are 1000 and 10,000, respectively. Given the weight of both, the training dataset can be considered as a small sample size. The default parameters of MIMO MC with drift system are shown in Table 1, and the values of parameters when used as variables, are given in the respective sections. The network parameters for channel KLD EGAN are shown in Table 2.

5.2. Generation capability analysis

In Fig. 6, the generation capability of the proposed KLD EGAN-based, original EGAN-based, and GAN-based learning methods is demonstrated. It should be noted that DNN and the two theoretical detectors are not analyzed here because they have no generation capability. In this paper, both the generator loss and discriminator loss of these three methods are taken into consideration. Since the minimax mutation loss function is applied in the original GAN, here, the same loss function displayed in (19) is selected as well for a fair comparison in both original EGAN and KLD EGAN.

The results show that there are still relatively severe oscillations in the GAN generator loss as the training epoch increases.

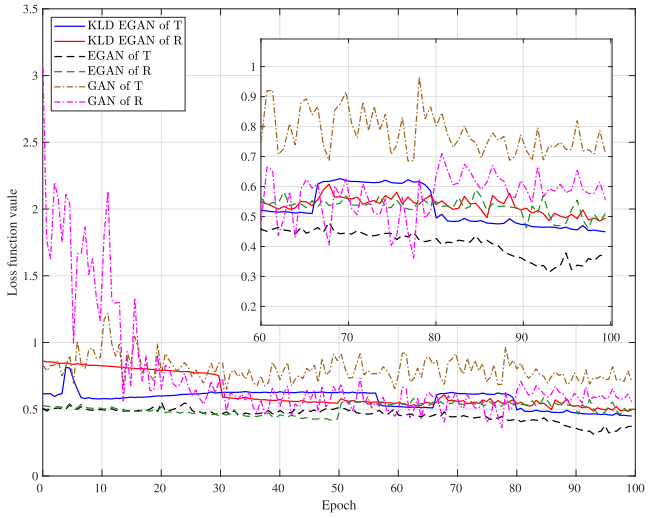

Fig. 6. Generation capability comparison between KLD EGAN, EGAN, and GAN when minimax mutation is selected.

This is due to the vanishing gradient and mode collapse of the GAN. In contrast, the generator losses of channel original EGAN and KLD EGAN are more stable, indicating that their generated signals have a higher degree of similarity to real received signals, showing better generation performance, and the KLD EGAN is superior. GAN will eventually reach Nash equilibrium in theory. In other words, the generator loss is equal to the discriminator loss, which is both 0.5. Also, results show that the two loss values of KLD EGAN are closer than that of GAN and original EGAN, both converging around 0.5, which means that it can generate more realistic MC channel data, leading to a positive contribution to the overall end-to-end signal recovery.

5.3. Model complexity analysis

Complexity analysis is important for resource-limited micro/nano machines in MC scenarios. Computational complexity is a measure of model complexity for online signal detection, and in this section, we will perform a simple theoretical analysis of five detectors and models. As mentioned before, W is the number of transceivers, and I is the length of the transmitted sequence. The computational complexity of the MAP detector can be expressed as $\mathcal{O}(2^{2W} \times I/W)$, while that of the FT detector is $\mathcal{O}(I)$, and the DNN-based, GAN-based, and KLD EGAN-based models are all $\mathcal{O}(I)$. It can be found that the computational complexity of the MAP detector increases exponentially with W. For the proposed KLD EGAN-based model, the computational complexity is the same as that of the sub-optimal FT detector, and both are relatively low. However, its BER performance is better than that of the FT detector in most cases.

Furthermore, as a data-driven approach, the training phase of the KLD EGAN-based model can be done in an offline manner, thus avoiding the periodic channel estimation process, which accounts for the extra overhead. More importantly, macro-scale devices can be used to facilitate complex offline training, which can then be transplanted to micro/nano-scale MC systems with lower computational power [43].

5.4. BER performance analysis

5.4.1. Signal-to-noise ratio

In order to evaluate the robustness of different detectors to the environment, Fig. 7 gives the BER performance of various models

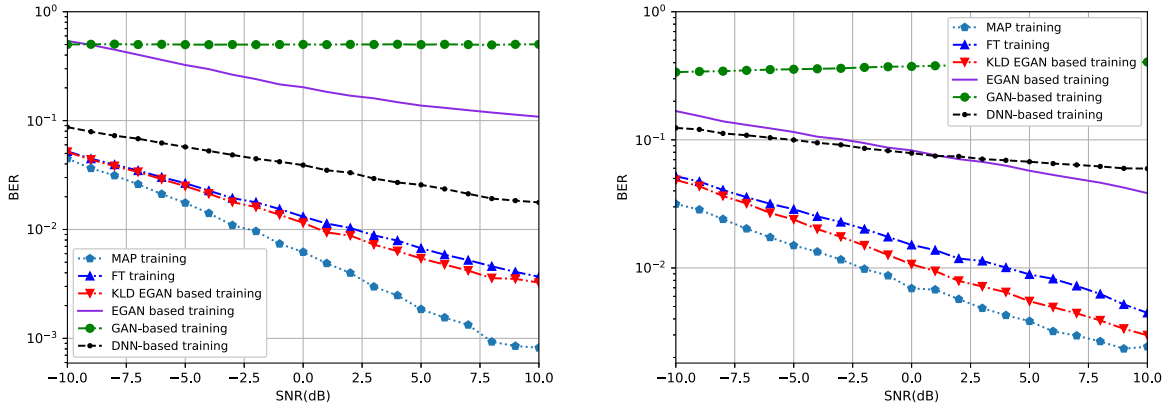

Fig. 7. Bit error rate performance comparison of SNR in MIMO molecular communication with drift system.

under different signal-to-noise ratios (SNR) by adjusting the noise variance σ_n, as shown in (29).

$$\mathrm{SNR} = 10 \cdot \log_{10}\left(\frac{N_s^2}{\sigma_n^2}\right), \tag{29}$$

where N_s and σ_n represent the power of signal and noise, respectively.

In this experiment, all models were trained on a noise-free channel, and during the test phase, the channel was operated with different intensities of Gaussian noise. It indicates that as SNR increases, the BER of all candidate models decreases. The BER of the proposed KLD EGAN-based model outperforms the sub-optimal FT detector and is second only to the optimal MAP detector. Also, compared with all other DL-based methods, the proposed KLD EGAN-based model is more robust for different SNRs, outperforming the DNN-based detector for which the channel is known and being second only to the optimal MAP detector. We also compared our proposed method with the original EGAN to demonstrate that the improved KLD mutation is effective. As shown in Fig. 7, the BER of KLD EGAN is lower than that of original EGAN at all SNR values. In addition, it is observed that the original GAN cannot converge in the case of a small training sample size. Due to the issues of vanishing gradient and mode collapse of GAN, training with signals extremely deviated from the real can cause incalculable damage to the end-to-end system.

Furthermore, the effect of ILI is more significant in the 3 × 3 MIMO system compared to 2 × 2, thus the optimal MAP detector, sub-optimal FT detector, and training-stable KLD EGAN-based model all have greater BERs in the 3 × 3 system. For example, at SNR=0 dB, the BER of MAP detector is 0.0062 under 2 × 2 MIMO but 0.0069 under 3 × 3 MIMO, and the BER of KLD EGAN-based model is 0.0094 under 2 × 2 MIMO but 0.0107 under 3 × 3 MIMO.

5.4.2. Molecules per bit

The effect of different numbers of molecules per bit on the BER performance for various models is shown in Fig. 8. With the number of molecules per bit rising, the uncertainty of Brownian motion is reduced, leading to a smaller effect of both ISI and ILI. Compared with other DL-based models, the proposed KLD EGAN-based model has a better BER performance, with a steady

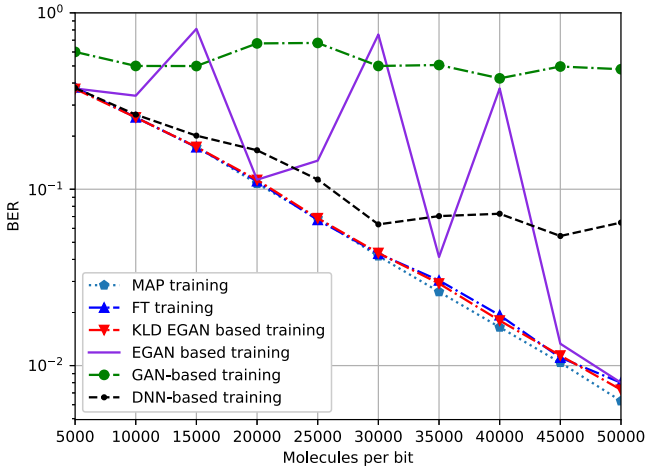

Fig. 8. Bit error rate performance comparison of molecules per bit in MIMO molecular communication with drift system.

decline as the number of molecules per bit increases. The BER performance of proposed KLD EGAN-based model outperforms the sub-optimal FT detector at all molecules per bit. Since both GAN and EGAN-based models are data-driven and are unknown to the underlying channel, the model that can more accurately simulate the underlying channel characteristics will have a lower BER value.

In addition, the BER curve of KLD EGAN-based model is smoother on all numbers of molecules per bit compared with the original EGAN-based and GAN-based models, indicating more stable training. Furthermore, there is a certain amount of oscillation for the DNN-based model since with the small training sample size the whole end-to-end system cannot be well trained.

5.4.3. Diffusion coefficient

The diffusion coefficient is also considered to be an essential parameter that will affect the performance of MIMO MC with drift system. As shown in Fig. 9, the BER increases with an increase in the diffusion coefficient. A larger diffusion coefficient means

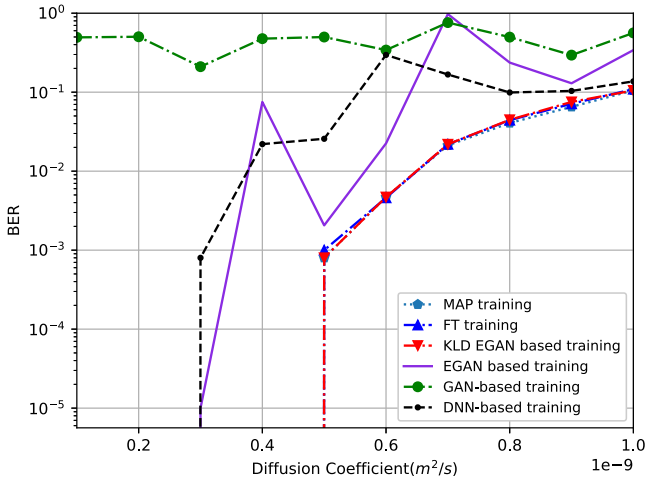

Fig. 9. Bit error rate performance comparison of diffusion coefficient in MIMO molecular communication with drift system.

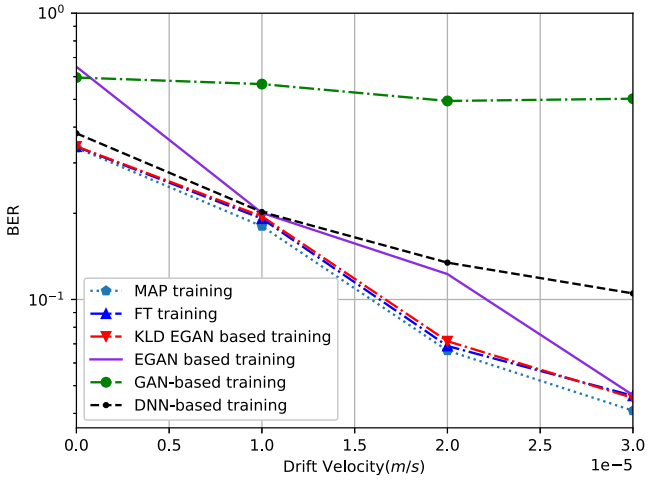

Fig. 10. Bit error rate performance comparison of dirft velocity in MIMO molecular communication with drift system.

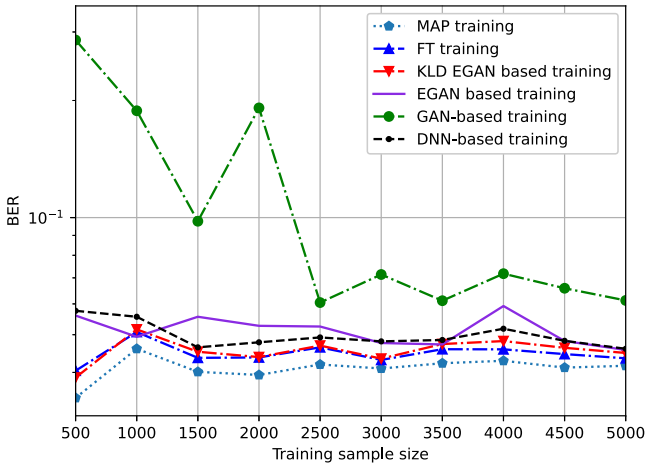

Fig. 11. Bit error rate performance comparison of training sample size in MIMO molecular communication with drift system.

higher randomness of the molecular Brownian motion, which may lead to an increase in both ISI and ILI effects. When the diffusion coefficient is less than 500 $\mu m^2/s$, the proposed KLD EGAN-based model can achieve zero BER performance, and the same is true of the optimal MAP and sub-optimal FT detectors. With the diffusion coefficient greater than 500 $\mu m^2/s$, the BER performance of KLD EGAN-based model is only second to the optimal MAP detector. It also outperforms all other DL-based methods with more stable training and better BER performance. In addition, both the original GAN-based and EGAN-based models show poor BER performance and oscillations under different parameters. This is because they cannot fit the signal distribution of the real channel well.

5.4.4. Dirft velocity

For MC systems with drift, the drift velocity is another parameter that cannot be ignored, affecting the molecules' transmission rate through the channel. As shown in Fig. 10, it is obvious that an increase in drift velocity leads to a decrease in the BER performance. It is quite reasonable that with a larger drift velocity, the effect of random molecular Brownian motion will be reduced, and the probability of reaching the corresponding receiver within the current time slot will increase. Adding additional drift to the MIMO MC system, both the effects of ISI and ILI can be suppressed considerably, as has been analyzed in Section 2.2. Thus the BER of the system can be reduced. When the drift velocity is zero, the proposed KLD EGAN-based detector is identical to the optimal detector. As the drift velocity increases, the proposed KLD EGAN-based detector continues to outperform the other DL-based detector. Similarly, the DNN-based model cannot train the end-to-end system well due to insufficient sample size. In contrast, the proposed KLD EGAN-based model is able to more accurately simulate the signal distribution of the real channel and thus achieve a lower BER.

5.4.5. Training sample size

Here, we discuss the impact of the training sample size on the signal recovery performance of MC system. With a smaller training size, the end-to-end system cannot learn the channel information well due to an insufficient sample size. However, the training data set can be expanded using a generative model. As shown in Fig. 11, at small training sets, e.g., 500, the proposed KLD EGAN-based method is second only to the optimal MAP detector since KLD EGAN can simulate the channel output distribution quite realistically and train the system with generated signals. While other DL-based methods show poor BER performance at this point, indicating that the complete information of channel cannot be learned well under this training sample set. As the training sample set increases, KLD EGAN-based method still outperforms all other DL-based methods.

6. Conclusion

In this paper, aiming at signal recovery of the newly developed mathematical MIMO MC with drift system model, a KLD EGAN-based end-to-end learning method is proposed. The additional drift term mitigates the effects of ISI for paired transceivers, ILI for unpaired transceivers, and other noise on the transmitted signal and thus reduces the transmission error. The proposed KLD EGAN-based method does not require an explicit channel model and can learn end-to-end link implicitly from the sampled data. Both the generated fake signals and real sampled signals are fed to the system for training signal detection. Results show that the BER performance of proposed channel KLD EGAN-based model outperforms the sub-optimal FT detector and is only second to the theoretical optimum MAP detector in most cases. In addition, KLD EGAN-based detector is superior to both GAN-based and original EGAN-based detectors in terms of channel output generation

capability and robustness to the environment, as it alleviates both problems mentioned above. Based on the proposed method, more realistic channel output can be generated for small training sample size cases, which helps to improve the signal recovery performance, thus making the MIMO MC system more robust to complex environments.

Our future research will primarily address channel estimation and the investigation of more end-to-end optimization methods based on MIMO MC with drift system. As for the experiments, we also plan to establish the experimental platform to verify the proposed mathematical model and proposed DL-based detection methods.

CRediT authorship contribution statement

Jiarui Zhu: Conceptualization, Methodology, Software, Investigation, Formal analysis, Writing – original draft. **Chenyao Bai:** Conceptualization, Funding acquisition, Resources, Supervision, Writing – review & editing. **Yunlong Zhu:** Conceptualization, Funding acquisition, Resources, Supervision, Writing – review & editing. **Xiwen Lu:** Resources, Supervision, Investigation. **Kezhi Wang:** Resources, Supervision.

Declaration of competing interest

The authors declare that they have no known competing financial interests or personal relationships that could have appeared to influence the work reported in this paper.

Data availability

No data was used for the research described in the article.

References

[1] L. Sun, Y. Wang, A.L. Swindlehurst, X. Tang, Generative-adversarial-network enabled signal detection for communication systems with unknown channel models, IEEE J. Sel. Areas Commun. 39 (1) (2020) 47–60.

[2] T. Nakano, Y. Okaie, J.-Q. Liu, Channel model and capacity analysis of molecular communication with Brownian motion, IEEE Commun. Lett. 16 (6) (2012) 797–800.

[3] M. Pierobon, I.F. Akyildiz, A physical end-to-end model for molecular communication in nanonetworks, IEEE J. Sel. Areas Commun. 28 (4) (2010) 602–611.

[4] S. Qiu, W. Guo, S. Wang, N. Farsad, A. Eckford, A molecular communication link for monitoring in confined environments, in: 2014 IEEE International Conference on Communications Workshops, ICC, IEEE, 2014, pp. 718–723.

[5] J. Chen, C.-L. Dong, D. Zhao, Y.-C. Huang, X. Wang, L. Samad, L. Dang, M. Shearer, S. Shen, L. Guo, Molecular design of polymer heterojunctions for efficient solar–hydrogen conversion, Adv. Mater. 29 (21) (2017) 1606198.

[6] U.A. Chude-Okonkwo, R. Malekian, B.T. Maharaj, A.V. Vasilakos, Molecular communication and nanonetwork for targeted drug delivery: A survey, IEEE Commun. Surv. Tutor. 19 (4) (2017) 3046–3096.

[7] B.-H. Koo, C. Lee, A.E. Pusane, T. Tugcu, C.-B. Chae, MIMO operations in molecular communications: Theory, prototypes, and open challenges, IEEE Commun. Mag. 59 (9) (2021) 98–104.

[8] C. Lee, B. Koo, N.-R. Kim, B. Yilmaz, N. Farsad, A. Eckford, C.-B. Chae, Molecular MIMO communication link, in: 2015 IEEE Conference on Computer Communications Workshops, INFOCOM WKSHPS, IEEE, 2015, pp. 13–14.

[9] B.-H. Koo, C. Lee, H.B. Yilmaz, N. Farsad, A. Eckford, C.-B. Chae, Molecular MIMO: From theory to prototype, IEEE J. Sel. Areas Commun. 34 (3) (2016) 600–614.

[10] O.A. Dambri, A. Abouaomar, S. Cherkaoui, Design optimization of a MIMO receiver for diffusion-based molecular communication, in: 2019 IEEE Wireless Communications and Networking Conference, WCNC, IEEE, 2019, pp. 1–6.

[11] T. Nakano, M.J. Moore, F. Wei, A.V. Vasilakos, J. Shuai, Molecular communication and networking: Opportunities and challenges, IEEE Trans. Nanobiosci. 11 (2) (2012) 135–148.

[12] H.B. Yilmaz, C.-B. Chae, Simulation study of molecular communication systems with an absorbing receiver: Modulation and ISI mitigation techniques, Simul. Model. Pract. Theory 49 (2014) 136–150.

[13] A. Noel, K.C. Cheung, R. Schober, D. Makrakis, A. Hafid, Simulating with AcCoRD: Actor-based communication via reaction–diffusion, Nano Commun. Netw. 11 (2017) 44–75.

[14] T. O'shea, J. Hoydis, An introduction to deep learning for the physical layer, IEEE Trans. Cogn. Commun. Netw. 3 (4) (2017) 563–575.

[15] D. García, J.O. Lacruz, D. Badini, D. De Donno, J. Widmer, Model-free machine learning of wireless SISO/MIMO communications, Comput. Commun. 181 (2022) 192–202.

[16] E. Zehavi, 8-PSK trellis codes for a Rayleigh channel, IEEE Trans. Commun. 40 (5) (1992) 873–884.

[17] Y. Wang, M. Liu, J. Yang, G. Gui, Data-driven deep learning for automatic modulation recognition in cognitive radios, IEEE Trans. Veh. Technol. 68 (4) (2019) 4074–4077.

[18] S. Peng, H. Jiang, H. Wang, H. Alwageed, Y. Zhou, M.M. Sebdani, Y.-D. Yao, Modulation classification based on signal constellation diagrams and deep learning, IEEE Trans. Neural Netw. Learn. Syst. 30 (3) (2018) 718–727.

[19] S. Ramjee, S. Ju, D. Yang, X. Liu, A.E. Gamal, Y.C. Eldar, Fast deep learning for automatic modulation classification, 2019, arXiv preprint arXiv:1901.05850.

[20] N.E. West, T. O'shea, Deep architectures for modulation recognition, in: 2017 IEEE International Symposium on Dynamic Spectrum Access Networks, DySPAN, IEEE, 2017, pp. 1–6.

[21] H. Huang, J. Yang, H. Huang, Y. Song, G. Gui, Deep learning for super-resolution channel estimation and DOA estimation based massive MIMO system, IEEE Trans. Veh. Technol. 67 (9) (2018) 8549–8560.

[22] H. Ye, G.Y. Li, B.-H. Juang, Power of deep learning for channel estimation and signal detection in OFDM systems, IEEE Wirel. Commun. Lett. 7 (1) (2017) 114–117.

[23] C.-K. Wen, S. Jin, K.-K. Wong, J.-C. Chen, P. Ting, Channel estimation for massive MIMO using Gaussian-mixture Bayesian learning, IEEE Trans. Wireless Commun. 14 (3) (2014) 1356–1368.

[24] S. Dörner, S. Cammerer, J. Hoydis, S. Ten Brink, Deep learning based communication over the air, IEEE J. Sel. Top. Sign. Proces. 12 (1) (2017) 132–143.

[25] F.A. Aoudia, J. Hoydis, Model-free training of end-to-end communication systems, IEEE J. Sel. Areas Commun. 37 (11) (2019) 2503–2516.

[26] H. Ye, G.Y. Li, B.-H.F. Juang, K. Sivanesan, Channel agnostic end-to-end learning based communication systems with conditional GAN, in: 2018 IEEE Globecom Workshops, GC Wkshps, IEEE, 2018, pp. 1–5.

[27] T.J. O'Shea, T. Erpek, T.C. Clancy, Physical layer deep learning of encodings for the MIMO fading channel, in: 2017 55th Annual Allerton Conference on Communication, Control, and Computing, Allerton, IEEE, 2017, pp. 76–80.

[28] J. Song, C. Häger, J. Schröder, T. O'Shea, H. Wymeersch, Benchmarking end-to-end learning of MIMO physical-layer communication, in: GLOBECOM 2020-2020 IEEE Global Communications Conference, IEEE, 2020, pp. 1–6.

[29] J. Song, C. Häger, J. Schröder, T.J. O'Shea, E. Agrell, H. Wymeersch, Benchmarking and interpreting end-to-end learning of MIMO and multi-user communication, IEEE Trans. Wireless Commun. (2022).

[30] Z. Sakkaff, J.L. Catlett, M. Cashman, M. Pierobon, N.R. Buan, M.B. Cohen, C.A. Kelley, End-to-end molecular communication channels in cell metabolism: An information theoretic study, in: Proceedings of the 4th ACM International Conference on Nanoscale Computing and Communication, 2017, pp. 1–6.

[31] C. de Vrieze, S. Barratt, D. Tsai, A. Sahai, Cooperative multi-agent reinforcement learning for low-level wireless communication, 2018, arXiv preprint arXiv:1801.04541.

[32] F.A. Aoudia, J. Hoydis, End-to-end learning of communications systems without a channel model, in: 2018 52nd Asilomar Conference on Signals, Systems, and Computers, IEEE, 2018, pp. 298–303.

[33] S. Mohamed, J. Dong, A. Junejo, et al., Model-based: End-to-end molecular communication system through deep reinforcement learning auto encoder, IEEE Access 7 (2019) 70279–70286.

[34] J. Song, B. Peng, C. Häger, H. Wymeersch, A. Sahai, Learning physical-layer communication with quantized feedback, IEEE Trans. Commun. 68 (1) (2019) 645–653.

[35] I. Goodfellow, J. Pouget-Abadie, M. Mirza, B. Xu, D. Warde-Farley, S. Ozair, A. Courville, Y. Bengio, Generative adversarial nets, Adv. Neural Inf. Process. Syst. 27 (2014).

[36] H. Ye, L. Liang, G.Y. Li, B.-H. Juang, Deep learning-based end-to-end wireless communication systems with conditional GANs as unknown channels, IEEE Trans. Wireless Commun. 19 (5) (2020) 3133–3143.

[37] C. Wang, C. Xu, X. Yao, D. Tao, Evolutionary generative adversarial networks, IEEE Trans. Evol. Comput. 23 (6) (2019) 921–934.

[38] V. Jamali, A. Ahmadzadeh, W. Wicke, A. Noel, R. Schober, Channel modeling for diffusive molecular communication—A tutorial review, Proc. IEEE 107 (7) (2019) 1256–1301.
[39] S. Das, P.N. Suganthan, Differential evolution: A survey of the state-of-the-art, IEEE Trans. Evol. Comput. 15 (1) (2010) 4–31.
[40] M. Wei, Perturbation of the least squares problem, Linear Algebra Appl. 141 (1) (1990) 177–182.
[41] D. Kilinc, O.B. Akan, Receiver design for molecular communication, IEEE J. Sel. Areas Commun. 31 (12) (2013) 705–714.
[42] B.H. Koo, H.B. Yilmaz, C.-B. Chae, A. Eckford, Detection algorithms for molecular MIMO, in: 2015 IEEE International Conference on Communications, ICC, IEEE, 2015, pp. 1122–1127.
[43] Y. Huang, F. Ji, Z. Wei, M. Wen, W. Guo, Signal detection for molecular communication: model-based vs. data-driven methods, IEEE Commun. Mag. 59 (5) (2021) 47–53.

Jiarui Zhu received her bachelor degree in computer science and technology from University of Geosciences in 2021. She is currently pursuing the master degree at the Academy for Engineering and Technology, Fudan University. Her research interests include the application of molecular communication and artificial intelligence.

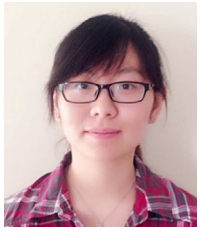

Chenyao Bai (Member, IEEE) received the B.Sc. degree in optical information science and technology from Shanxi University, China, in 2011, and M.Sc. and Ph.D. degrees in communications engineering from the University of Warwick, UK, in 2012 and 2016, respectively. She is currently a Postdoctoral Research Fellow with Fudan University, China, with the Academy for Engineering & Technology. Her research interests include molecular communication, quorum sensing, machine learning and targeted drug delivery.

Yunlong Zhu received the Ph.D. degree in mechatronic engineering from the Shenyang Institute of Automation, Chinese Academy of Sciences, Shenyang, China, in 2005. He is currently a Distinguished Professor with Fudan University, China, with the Academy for Engineering & Technology. His research interests include data/knowledge driven swarm intelligence computational modeling, industrial sensor network and edge computing, industrial internet of things, interconnected intelligent factory, and ultra-precise flexible OLED electronic printing technology and equipment.

Xiwen Lu received his Bachelor degree in Computer Science from the China University of Mining and Technology, in 2021. He is currently pursuing his Ph.D. degree directly at the Academy for Engineering and Technology, Fudan University. His research interests include the application of artificial intelligence and biological nanorobots.

Kezhi Wang received Ph.D. degree in Engineering from the University of Warwick, U.K. He was with University of Essex and Northumbria University, U.K. Currently he is a Senior Lecturer with Department of Computer Science, Brunel University London, U.K. His research interests include wireless communications, signal processing, mobile edge computing and machine learning. He is a co-recipient of the IEEE ComSoc Leonard G. Abraham Prize in 2022.